Journal of Power Sources 210 (2012) 158–162

Contents lists available at SciVerse ScienceDirect

Journal of Power Sources

journal homepage: www.elsevier.com/locate/jpowsour

Ca_7Ge-type hydride $Mg_6VNa_xH_y$ ($0 \leq x \leq 1$): High pressure synthesis, synchrotron X-ray analysis and hydrogen storage properties

N. Takeichi, J. Yan, X. Yang, K. Shida, H. Tanaka, T. Kiyobayashi*, N. Kuriyama, T. Sakai

Research Institute for Ubiquitous Energy Devices, National Institute of Advanced Industrial Science and Technology (AIST), 1-8-31 Midorigaoka, Ikeda, Osaka 563-8577, Japan

ARTICLE INFO

Article history:
Received 14 December 2011
Received in revised form 6 March 2012
Accepted 8 March 2012
Available online 21 March 2012

Keywords:
High pressure
Hydrogen storage
Rietveld analysis
Synchrotron X-ray

ABSTRACT

A powder mixture of MgH_2:VH_2:NaH = 6:1:*n* is treated under 8 GPa at 873 K using an eight-anvil apparatus in order to investigate the influence of NaH addition to Mg_6VH_y, a Ca_7Ge-type FCC hydride. Synchrotron radiation X-ray diffraction (SR-XRD) of the obtained sample reveals that Na occupies the vacant 4b site in Mg_6VH_y to form $Mg_6VNa_xH_y$ ($0 \leq x \leq 1$) as the main product while retaining its Ca_7Ge-type structure. The Rietveld analysis of the SR-XRD data suggests that the bond lengths between hydrogen and magnesium remain constant through the Na addition. All the samples reversibly desorb and absorb hydrogen at 620–630 and 590–600 K, respectively, under 0.5 MPa (H_2). These temperatures are, respectively, about 70 and 120 K lower than those of MgH_2. The hydrogen capacity of the main product phase, $Mg_6VNa_xH_y$, is estimated to be 5–6 mass% from the pressure-composition isotherms (PCIs) by taking its content rate in the specimen into account. The reaction enthalpies calculated from the van't Hoff relation of the PCIs do not significantly differ from that of MgH_2. The bond lengths and energies between hydrogen and magnesium are not affected by the perturbation by the NaH addition in the lattice in $Mg_6VNa_xH_y$.

1. Introduction

Magnesium has long been a candidate element for hydrogen storage because its hydiride, MgH_2, contains a large amount of hydrogen, 7.6 mass% [1]. However, the high thermodynamic stability and sluggish reaction kinetics of MgH_2 require a high working temperature, *e.g.*, ~700 K, to absorb and desorb hydrogen, limiting its practical application as a hydrogen storage material. Recently, MgH_2 combined with a small amount of catalysts, metals, metal oxides and carbons have been investigated [2–10], some of which desorbed hydrogen at the temperatures about 100 K lower than that of pristine MgH_2. High absorption rates were observed even at room temperatures [6,10]. Other efforts to overcome the drawback of Mg-based materials are: elemental substitution [11,12], mechanical alloying [13,14], laminate composites [15,16], vapor phase processing [17], combustion synthesis [18,19], *etc.*

Applying a high pressure to metals in the presence of hydrogen is another option to develop hitherto unknown Mg-based hydrides that cannot be formed under ambient conditions. This is because the chemical potential of gaseous hydrogen significantly increases above 1 GPa and consequently the solubility of hydrogen in metals significantly increases [20]. Especially, by using hydrides instead of pure metals as precursors, one can synthesize hydrides not only of known alloys [21], but also of which the fully dehydrogenated state cannot be found in the phase diagram. Based on this methodology, many Mg-rich hydrides have been discovered by Okada et al. of Tohoku University [22–25] and by us [26–33]. Many of these hydrides desorb hydrogen at lower temperatures than MgH_2. Besides, some of them reversibly absorb and desorb hydrogen under ambient pressure. In relation to the present study, we found that the systems M = Ti and V formed $Mg_{6\sim7}MH_y$, a face-centered cubic (FCC) structure as a stable main phase under 8 GPa at 873 K [26–28]. Although both systems belong to the same Ca_7Ge-type structure, while the Ti-system forms Mg_7TiH_y with all the sites for the metal elements occupied, the major product in the V-system is Mg_6VH_y with one site (4b) left vacant even if the initial ratio of Mg to V is 7:1. The addition of Na into Mg_7TiH_y results in the replacement of Mg with Na accompanied by structural phase transitions. The initially poor reversibility of the hydrogen absorption and desorption is significantly improved by the alkaline metal addition [34,35].

In the present study, we investigated the effect of the Na-addition for Mg_6VH_y by comparing it to Mg_7TiH_y on the fundamental research basis. Points of the argument are:

(i) Does Na replace Mg in Mg_6VH_y as in Mg_7TiH_y, or does it occupy the vacant site in Mg_6VH_y that is not available in Mg_7TiH_y?
(ii) Does Na influence the hydrogen storage properties of Mg_6VH_y?

* Corresponding author. Tel.: +81 72 751 9651; fax: +81 72 751 9629.
E-mail address: kiyobayashi-t@aist.go.jp (T. Kiyobayashi).

0378-7753/$ – see front matter © 2012 Elsevier B.V. All rights reserved.
doi:10.1016/j.jpowsour.2012.03.034

We processed the powder mixture of MgH_2, VH_2 and NaH with molar ratios of 6:1:n (n = 0, 0.3, 0.7 and 1.0) under 8 GPa at 873 K. The obtained samples were subjected to synchrotron radiation X-ray diffraction (SR-XRD) to determine the crystal structure and hydrogen positions based on a Rietveld analysis. The hydrogen desorption and absorption properties were examined by thermal analysis and pressure-composition isotherm (PCI) measurements.

2. Experimental

The high pressure synthesis applied in our present and previous studies is based on the technique developed by Fukai et al. [36,37]. As mentioned in the Introduction, a feature of our high pressure synthesis is to use metal hydrides as the starting materials instead of pure metals. Powders of MgH_2 (nominal purity 98%), VH_2 (99.9%) and NaH (95%) were purchased from Alfa Aesar, Mitsuwa and Aldrich, respectively, and used without further purification. All the materials were handled in a glove box filled with Ar of which the dew-point and oxygen concentration were maintained below 200 K and 1 ppm. MgH_2, VH_2 and NaH were mixed in the molar ratios of MgH_2:VH_2:NaH = 6:1:n where n = 0, 0.3, 0.7 and 1.0. The powder mixture (45 mg) was pressed into a 4-mm diameter pellet. The details of the high pressure synthesis are described in our previous studies [27,33]. The pellets and anvils assembly was compressed under 8 GPa at 873 K for 1 h using a high-pressure generating machine (UHP-2000, Sumitomo Heavy Industries). Prior to the high pressure synthesis in the present study, the pressure gauge was calibrated by observing the shift in the electrical resistance of Bi and Ba placed in the anvil assembly; these metals are known to undergo pressure-induced phase transitions Bi(I) to Bi(II), Ba(I) to Ba(II) and Bi(V) to Bi(VII) at 2.6, 5.5 and 7.7 GPa, respectively, at room temperature.

The sample processed at the high pressure was examined by powder X-ray diffractometry at the beam line BL19B2 in the synchrotron radiation facility SPring-8, Japan. The Debye–Scherrer camera (radius: 286.5 mm) was equipped with an imaging plate (pixel size: 50 μm) on the 2θ-arm as a detector. In the present study, the diffraction angle range was $3 < 2\theta/\mathrm{deg} < 77$ and one scan took five minutes. The wavelength of the monochromatic X-ray was calibrated to be λ/Å = 0.70067(1) using a CeO_2 crystal, a/Å = 5.41134, as the reference. The sample powder was contained in a glass capillary (0.3 mm outer diameter) and sealed with an epoxy-resin adhesive in the Ar glove box.

The crystal structure was analyzed by the Rietveld refinement program RIETAN-FP [38]. A split pseudo-Voigt function was used as the profile function. The sequence of the parameter optimization is as follows: (1) parameters of the profile function of each phase, (2) lattice constants and occupancy of Na (for $n > 0$), (3) fractional coordinates of H atoms firstly with and then without "soft constraint" on the H atoms, (4) isotropic thermal displacement factors B of the metallic elements and (5) B's of the H atoms. The Rietveld analysis was carried out on the XRD patterns in Fig. 1 in Section 3.1 based on the structure model presented in Section 3.2. The main Ca_7Ge-type phase product as well as the minor unreacted and impurity phases, α-MgH_2, γ-MgH_2, VH_2, V_2H, MgO and NaCl, were simultaneously refined, in which NaCl is an impurity resulting from the rock-salt capsule for the high pressure synthesis.

The hydrogen desorption and absorption properties were investigated by a differential scanning calorimeter (DSC, DSC-8230HP, Rigaku) under the hydrogen pressure of 0.5 MPa with the heating and cooling rates of 10 K min^{-1}. The pressure-composition isotherms (PCIs) were determined using a gas-volumetric apparatus (PCT-A08-01, LESCA). The sample, ca. 20 mg, was first dehydrogenated by evacuating at 573 K below 100 Pa. After the dehydrogenation, the PCIs were measured at 523, 548 and 573 K under an equilibrium hydrogen pressure from 100 Pa to 0.8 MPa.

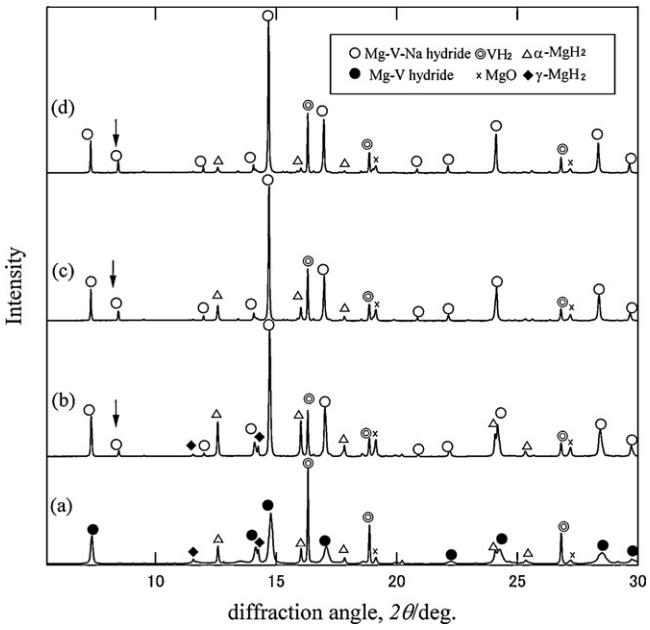

Fig. 1. Synchrotron X-ray diffraction patterns of $6MgH_2$ +VH_2 +nNaH treated under 8 GPa at 873 K. n = (a) 0, (b) 0.3, (c) 0.7 and (d) 1.0. Reflection indicated by the arrow is from the (2 0 0) plane of the Ca_7Ge structure, testifying to the occupation of the 4b site by an atom.

3. Result and discussion

3.1. Crystallographic structure

Fig. 1 shows the SR-XRD patterns of the mixtures $6MgH_2$ +VH_2 +nNaH processed under 8 GPa at 873 K for 1 h. As in our previous studies on the Mg–Ti [35] and Mg–V [28] systems, reflections that are well indexed by the FCC structure are predominantly observed along with impurities and the starting materials except for NaH. For n = 0, the diffractions from the FCC phase agreed well with our previous study [28]; *viz.*, the FCC phase is expressed as Mg_6VH_y with the Ca_7Ge-type structure belonging to the space group $Fm\bar{3}m$ in which Mg and V occupy the 24d and 4a sites, respectively, and the 4b site is left vacant.

When NaH was added to the starting mixture ($n > 0$), a diffraction peak marked by the arrow in Fig. 1, which is absent for n = 0, grew in intensity with the increasing amount of NaH. In the Ca_7Ge-type, this reflection appears only if the 4b site is occupied by an atom (reflection from (2 0 0) plane). This observation and the fact that no NaH was observed in the product suggest that Na atoms added to Mg_6VH_y are probably incorporated into the vacant 4b site. We will discuss the position of Na in detail by the Rietveld modeling as described below.

3.2. Rietveld analysis

The purpose of the Rietveld structure analysis in the present study is (i) to verify the above mentioned hypothesis about the position of Na and (ii) to locate the H atom in the lattice. The laboratory-scale X-ray used in our previous study [28] prohibited task (ii). Only with the high brilliance of the SR-XRD was it undertaken in the present study.

The model structure is summarized in Table 1 and Fig. 2. As mentioned in the previous section, we hypothesized that Na occupies the 4b site which is vacant if no NaH is added. There are two conceivable tetrahedral sites for H to occupy, both being labeled 32f; one is surrounded by one V atom in the 4a site and three Mg atoms

Table 1
Model structure for the Rietveld refinement of $Mg_6VNa_xH_y$.

Atom	Site	Occupancy	Coordinates		
			X	*Y*	*Z*
V	4a	1.0	0	0	0
Na	4b	*x*	1/2	1/2	1/2
Mg	24d	1.0	0	1/4	1/4
H(1)	32f	1.0	h_1	h_1	h_1
H(2)	32f	1.0	h_2	h_2	h_2

in the 24d site, termed H(1), and the other by one vacancy or Na atom in the 4b site and three Mg atoms in the 24d site, H(2).

The result of the analysis pertinent to the discussion is summarized in Table 2. Fig. 3 shows the refined XRD profile of the sample $n = 1.0$ (Fig. 1(d)) as an example of the refinement. The *R*-factors of the weighted pattern, R_{wp}, of the Rietveld refinement were 9–11%. The ratio of R_{wp} to R_e, $S \equiv R_{wp}/R_e$, where R_e determines the theoretical lower limit of the *R*-factor, converged to <2.5, which we consider satisfactory as a refinement of multi-phase hydrogen-containing materials.

As Table 2 shows, the content rate, *C*, of the Ca_7Ge-type structure tends to increase when more NaH is added. This coincides with our previous observation that the addition of an alkali metal species, such as $LiAlH_4$, can improve the yield of the target phase in the high pressure synthesis [34,35].

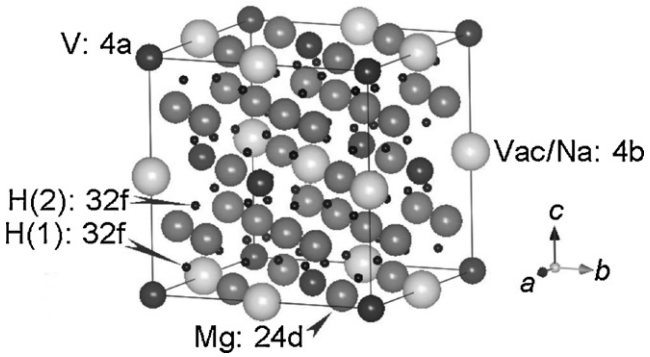

Fig. 2. Atomic arrangement in the model structure for the Rietveld refinement of $Mg_6VNa_xH_y$.

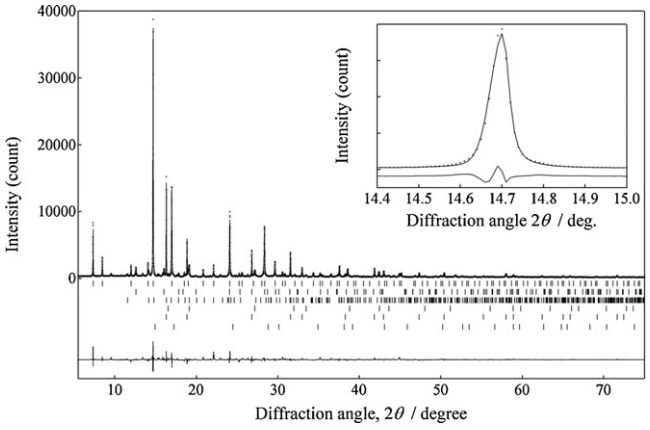

Fig. 3. Refined XRD profile of the sample $6MgH_2 + VH_2 + 1.0NaH$ treated under 8 GPa at 873 K. Bars below the profile indicate, from top to bottom, the positions of reflection from the Ca_7Ge-type model structure $Mg_6VNa_xH_y$, α-MgH_2, γ-MgH_2, MgO, VH_2 and NaCl, respectively. The lowermost signal indicates the residue of the experimental profile subtracted by the refined one. The inset magnifies the profile around 2θ/deg = 14.7 where the highest intensity peak is located.

The occupancy of Na at the 4b site, *x*, also monotonously increased upon the NaH-addition. Accordingly, so did the lattice constant, *a*, of the Ca_7Ge-type. The lattice expansion can be understood by the fact that the Goldschmidt radius of Na, 1.86 Å, is larger than those of Mg, 1.60 Å, and V, 1.32 Å. The $Mg_6VNa_xH_y$ phase, however, retained its cubic structure even if almost all the vacant 4b sites were filled with Na (*x* reached to 0.96 when $n = 1.0$), which stands in marked contrast to the case for the Mg–Ti system. For the Mg–Ti system, the main product of the high pressure synthesis is Mg_7TiH_y where all the 4b sites are already occupied together with the 24d sites by Mg [34]. The addition of Na to Mg_7TiH_y leads to the replacement of Mg with Na along with concomitant structural phase transitions first from cubic to tetragonal and eventually to monoclinic [35].

As for the positions of hydrogen, if H(1) and H(2) were exactly situated at the center of the tetrahedron of the 32f site, h_1 and h_2 would be 1/8 and 3/8, respectively. That $h_1 < 1/8$ and $h_2 < 3/8$ suggests that, regardless of the Na content, H(1) is off-centered toward a V atom (4a), while H(2) tends to stay away from a vacancy/Na atom (4b). The distances between H and the metal elements at $x = 0$ in the present study roughly coincide with the *ab initio* modeling of Mg_6VH_{16} by Shelyapina et al. who calculated the above distances to be d/Å = 1.779, 2.169, 2.385 and 1.974 for H(1)-V, H(1)-Mg, H(2)-Vac and H(2)-Mg, respectively [39]. One can notice that the distances between H and Mg are by and large constant regardless of the Na content. The tendency to maintain constant distances between H and Mg was also observed in Mg_7TiH_y with Li addition; *i.e.*, the distances calculated by the authors of the present study from the XRD data given in Ref. [34] are d/Å ~1.6, 2.3, 2.3 and 2.0 for H(1)-Ti, H(1)-Mg in 24d, H(2)-Mg/Li in 4b and H(2)-Mg in 24d, respectively, in the Li load range of $n = 0 \sim 0.3$.

3.3. Reaction with hydrogen

All the samples, including the one without Na-addition $n = 0$, underwent reversible hydrogen desorption and absorption cycles at 0.5 MPa of hydrogen in the DSC as suggested by an endothermic effect during the heating process and an exothermic one during the cooling. Fig. 4 shows the initial five cycles of the DSC signal for $n = 1.0$ as a representative example. This is in contrast to Mg_7TiH_y of which the reversibility was not satisfactory. Only by adding alkaline metals did the Mg–Ti system gain the reversible reactivity with hydrogen [34]. Fig. 5 shows the DSC peaks of the samples prepared in the present study as well as those of MgH_2 for comparison. The amount of Na, *n*, does not prominently influence the reaction temperatures; *i.e.*, at any Na content, the peak onset temperatures of the hydrogen desorption, Fig. 5(a), and absorption, (b), are 620–630 and 590–600 K, respectively, which are around 70 and 120 K lower than those of MgH_2. The fact that both the desorption

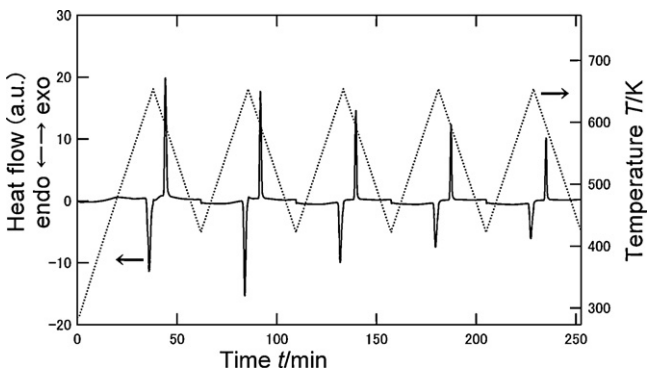

Fig. 4. Initial five DSC cycles of heating and cooling at 0.5 MPa of hydrogen. Sample: $6MgH_2 + VH_2 + 1.0NaH$ treated under 8 GPa at 873 K.

Table 2
Result of the Rietveld refinement of $Mg_6VNa_xH_y$ with Ca_7Ge structure (FCC, $Fm\bar{3}m$) synthesized from $6MgH_2$ +VH_2 +nNaH treated under 8 GPa at 873 K.

	n			
	0.0	0.3	0.7	1.0
Content rate, C/ wt.%	57.7	60.4	65.9	75.2
Lattice constant, a/Å	9.4293(5)	9.4502(2)	9.4562(2)	9.4834(2)
Occupancy of Na in 4b, x	0.0	0.67	0.86	0.97
Position of H(1) in 32f, h_1	0.117	0.092	0.094	0.099
of H(2) in 32f, h_2	0.374	0.374	0.356	0.358
Distance d(H(1)-V)/Å	1.91(4)	1.51(1)	1.54(1)	1.63(2)
d(H(1)-Mg)/Å	2.10(1)	2.28(3)	2.26(2)	2.23(2)
d(H(2)-Vac/Na)/Å	2.05(2)	2.06(2)	2.35(2)	2.33(2)
d(H(2)-Mg)/Å	2.03(2)	2.04(2)	1.96(2)	1.97(2)
B(V)/Å^2	0.68(2)	0.76(2)	0.51(4)	0.48(3)
B(Na)/Å^2	–	1.3(1)	2.4(1)	1.3(1)
B(Mg)/Å^2	1.95(8)	2.55(3)	2.91(5)	2.23(4)
B(H(1 and 2))/Å^2	3.9(1)	3.6(2)	3.5(2)	3.1(2)
R_I/%	2.35	1.76	2.64	3.60
R_F/%	1.39	2.21	3.65	1.71
R_{wp}/%	8.55	8.62	11.42	10.48
R_e/%	4.16	4.12	4.74	4.76
$S \equiv R_{wp}/R_e$	2.06	2.09	2.41	2.20

B: Isotropic thermal displacement factor; R: R-factor (I: integrated intensity, F: structure, wp: weighted pattern, e: expected). All phases under consideration are involved in R_{wp} and R_e.

and absorption temperatures are lower than those of MgH_2 suggests that the observed reversible reactions with hydrogen in the DSC stem from $Mg_6VNa_xH_y$, not from MgH_2 remaining in the sample as an impurity. The peak area of the hydrogen absorption of the present sample is close to that of the desorption, indicating the better reversibility than MgH_2 of which the absorption peak area is much smaller than the desorption due to the poor reversibility.

The PCIs of $Mg_6VNa_xH_y$ at 573 K are shown in Fig. 6. Due to the small amount (ca. 20 mg) of the specimen available for the measurement, the precision of the PCIs is, unfortunately, not very satisfactory, so that the discussion below is mostly speculative. The maximum hydrogen contents in the samples range from 3 to 4 mass%. Considering that the by-products in the samples, MgH_2, VH_2, MgO, *etc.*, do not absorb or desorb hydrogen under the PCI measurement conditions, we can assume that the observed hydrogen content is attributed to the $Mg_6VNa_xH_y$ phase. By taking into account the content ratio C of the $Mg_6VNa_xH_y$ phase in the specimen (see Table 2), the hydrogen content in $Mg_6VNa_xH_y$ is estimated to be 5–6 mass%, which is about 80–90% of the nominal hydrogen content of 6–8 mass% in $Mg_6VNa_xH_y$ with y = 14–16. In general, certain hydrides lose their reversibility for hydrogen storage when they are completely dehydrogenated; *i.e.*, the hydrides retain their reversibility only in the range $a \le y \le b$ with $0 < a$ in the formula MH_y and the hydrogen in $0 \le y \le a$ is "stored away". The above observation that the reversible hydrogen content does not reach the nominal content may suggest that a certain amount of hydrogen must be stored away in order to sustain the structure and reversibility of $Mg_6VNa_xH_y$. A more precise examination is necessary for any further discussions.

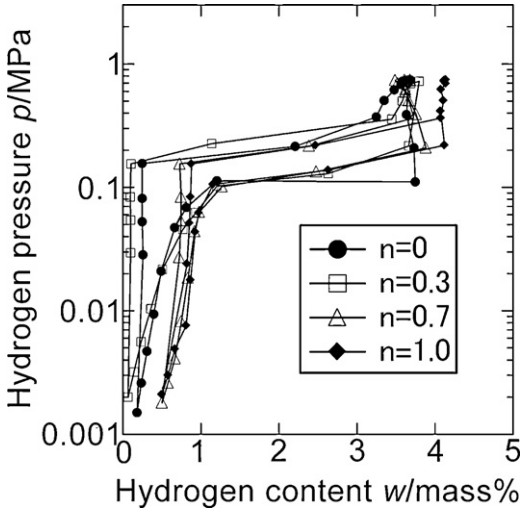

Fig. 6. The pressure-composition isotherms (PCIs) at 573 K of the sample $6MgH_2$ +VH_2 +nNaH treated under 8 GPa at 873 K.

From the slope of the van't Hoff plot, $\ln p$ vs. $1/T$, using PCIs measured at 523, 548 and 573 K (not shown), the reaction enthalpy was calculated to be $|\Delta H|$/kJ mol$(H_2)^{-1}$ = 71–77 regardless of the Na content, which does not significantly differ from that of MgH_2, $|\Delta H|$/kJ mol$(H_2)^{-1}$ = 74 [1]. For the transition metal alloys, the shift in the lattice lengths often correlates well with the enthalpies of reaction with hydrogen, for example as in Ref. [40]. On the other

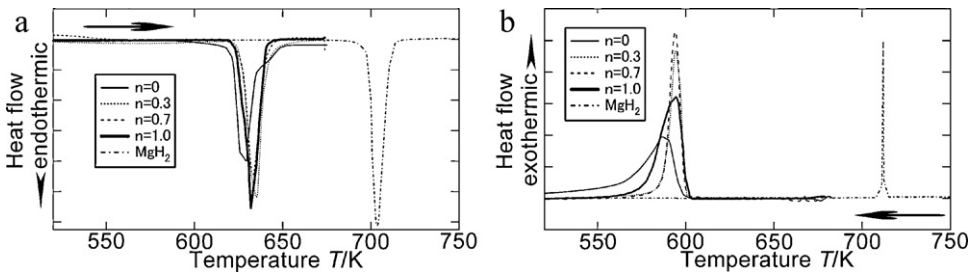

Fig. 5. The DSC signals of the samples $6MgH_2$ +VH_2 +nNaH treated under 8 GPa during the heating (a) and cooling (b) processes, compared to MgH_2. The peaks are suggested to reflect the hydrogen desorption and absorption of the Ca_7Ge-type phase, $Mg_6VNa_xH_y$.

hand, the bonding energy between H and Mg, a typical element, seems to be independent of the lattice lengths so long as the content of Mg in the alloy is high as in Mg_6VH_y or Mg_7TiH_y. Shao et al. revealed that the remarkably enhanced reactivity of their nano-structured MgH_2/TiH_2 composite is purely due to the kinetics and not to the thermodynamics [10]. The lower reaction temperatures of Mg_7TiH_y and $Mg_6VNa_xH_y$ than pristine MgH_2 may not result from the thermodynamic change of the materials, but from a catalytic effect of constituent elements such as Ti or V. Further investigation is required to fathom the reaction mechanism of Mg-based materials synthesized by high pressure techinique; *e.g.,* tracking how the phases change through many cycles of hydrogen desorption and absorption.

4. Conclusions

The synchrotron radiation X-ray diffraction (SR-XRD) and the Rietveld analysis revealed that:

- Applying 8 GPa of pressure to the powder mixture of MgH_2:VH_2:NaH = 6:1:n at 873 K for 1 h results in a Ca_7Ge-type hydride, $Mg_6VNa_xH_y$.
- The addition of NaH increases the content rate (yield) of the $Mg_6VNa_xH_y$ phases.
- Na occupies the 4b site, which is left vacant in Mg_6VH_y, accompanied by a monotonous expansion of the lattice according to the Na content without any structural phase transitions. The result is in contrast to Mg_7TiH_y which has no vacancy left for Na, and undergoes structural phase transitions by replacing Mg with Na.
- H occupies two positions in the 32f site. The distances between H and Mg remain constant despite the expansion in the lattice upon Na addition.

$Mg_6VNa_xH_y$ reversibly desorbs and absorbs hydrogen. The reversible capacity is estimated to be 5–6 mass%. The temperatures of dehydrogenation and hydrogenation of $Mg_6VNa_xH_y$ are about 70 and 120 K lower than those of MgH_2. However, the reaction enthalpy of $Mg_6VNa_xH_y$, estimated to be 71–77 kJ mol$(H_2)^{-1}$, does not significantly differ from that of MgH_2.

References

[1] J.F. Stampfer Jr., C.E. Holley Jr., J.F. Suttle, J. Am. Chem. Soc. 82 (1960) 3504–3508.
[2] A. Zaluska, L. Zaluski, J.O. Ström-Olsen, J. Alloys Compd. 288 (1999) 217–225.
[3] W. Oelerich, T. Klassen, R. Bormann, J. Alloys Compd. 315 (2001) 237–242.
[4] W. Oelerich, T. Klassen, R. Bormann, J. Alloys Compd. 322 (2001) L5–L9.
[5] G. Barkhordarian, T. Klassen, R. Bormann, Scripta Mater. 49 (2003) 213–217.
[6] N. Hanada, T. Ichikawa, S. Hino, H. Fujii, J. Alloys Compd. 420 (2006) 46–49.
[7] M.A. Lillo-Ródenas, Z.X. Guo, K.F. Aguey-Zinsou, D. Cazoria-Amorós, A. Linares-Solano, Carbon 46 (2008) 126–137.
[8] A. Chaise, P. de Rango, Ph. Marty, D. Fruchart, S. Miraglia, R. Olivès, S. Garrier, Int. J. Hydrogen Energy 34 (2009) 8589–8596.
[9] R.K. Singh, H. Raghubanshi, S.K. Pandey, O.N. Srivastava, Int. J. Hydrogen Energy 35 (2010) 4131–4137.
[10] H. Shao, M. Felderhoff, F. Schüth, Int. J. Hydrogen Energy 36 (2011) 10828–10833.
[11] J.J. Reilly, R.H. Wiswall Jr., Inorg. Chem. 6 (1967) 2220–2223.
[12] J.J. Reilly, R.H. Wiswall Jr., Inorg. Chem. 7 (1968) 2254–2256.
[13] M.Y. Song, Int. J. Hydrogen Energy 20 (1995) 221–227.
[14] K.J. Gross, P. Spatz, A. Züttel, L. Schlapbach, J. Alloys Compd. 240 (1996) 206–213.
[15] T.T. Ueda, M. Tsukahara, Y. Kamiya, S. Kikuchi, J. Alloys Compd. 386 (2005) 253–257.
[16] N. Takeichi, K. Tanaka, H. Tanaka, T.T. Ueda, Y. Kamiya, M. Tsukahara, H. Miyamura, S. Kikuchi, J. Alloys Compd. 446–447 (2007) 543–548.
[17] S.E. Guthrie, G.J. Thomas, in: H.S. Kliger (Ed.), Proc. 43rd International SAMPE Symposium, Advancement of Materials and Process Engineering, vol. 43, Covina, 1998, pp. 1105–1112.
[18] H. Isogai, T. Akiyama, J. Yagi, J. Jpn. Inst. Met. 60 (1996) 338–344.
[19] T. Akiyama, H. Isogai, J. Yagi, J. Alloys Compd. 252 (1997) L1–L4.
[20] Y. Fukai, The Metal-Hydrogen System: Basic Bulk Properties, Springer, Berlin, 2005.
[21] B. Bertheville, K. Yvon, J. Alloys Compd. 290 (1999) L8–L10.
[22] H. Takamura, H. Kakuta, A. Kamegawa, M. Okada, J. Alloys Compd. 330–332 (2002) 157–161.
[23] A. Kamegawa, Y. Goto, H. Kakuta, H. Takamura, M. Okada, J. Alloys Compd. 408–412 (2006) 284–287.
[24] M. Okada, Y. Goto, R. Kataoka, Y. Yambe, A. Kamegawa, H. Takamura, J. Alloys Compd. 446–447 (2007) 6–10.
[25] R. Kataoka, Y. Goto, A. Kamegawa, H. Takamura, M. Okada, J. Alloys Compd. 446–447 (2007) 142–146.
[26] D. Kyoi, T. Sato, E. Rönnebro, N. Kitamura, A. Ueda, M. Ito, S. Katsuyama, S. Hara, D. Noréus, T. Sakai, J. Alloys Compd. 372 (2004) 213–217.
[27] E. Rönnebro, D. Kyoi, A. Kitano, Y. Kitano, T. Sakai, J. Alloys Compd. 404 (2005) 68–72.
[28] D. Kyoi, T. Sato, E. Rönnebro, Y. Tsuji, N. Kitamura, A. Ueda, M. Ito, S. Katsuyama, S. Hara, D. Noréus, T. Sakai, J. Alloys Compd. 375 (2004) 253–258.
[29] T. Sato, D. Kyoi, E. Rönnebro, N. Kitamura, T. Sakai, D. Noréus, J. Alloys Compd. 417 (2006) 230–234.
[30] D. Kyoi, N. Kitamura, H. Tanaka, A. Ueda, S. Tanase, T. Sakai, J. Alloys Compd. 428 (2007) 268–273.
[31] D. Kyoi, T. Sakai, N. Kitamura, A. Ueda, S. Tanase, J. Alloys Compd. 463 (2008) 306–310.
[32] D. Kyoi, T. Sakai, N. Kitamura, A. Ueda, S. Tanase, J. Alloys Compd. 463 (2008) 311–316.
[33] T. Takasaki, D. Kyoi, N. Kitamura, S. Tanase, T. Sakai, J. Phys. Chem. B 111 (2007) 14102–14106.
[34] T. Takasaki, T. Mukai, N. Kitamura, S. Tanase, T. Sakai, J. Phys. Chem. B 112 (2008) 12540–12544.
[35] T. Takasaki, T. Mukai, N. Kitamura, S. Tanase, T. Sakai, J. Alloys Compd. 494 (2010) 439–445.
[36] Y. Fukai, N. Okuma, Jpn. J. Appl. Phys. 32 (1993) L1256–L1259.
[37] Y. Fukai, Y. Ishii, Y. Goto, K. Watanabe, J. Alloys Compd. 313 (2000) 121–132.
[38] F. Izumi, K. Momma, Solid State Phenom. 130 (2007) 15–20.
[39] M.G. Shelyapina, D. Fruchart, P. Wolfers, Int. J. Hydrogen Energy 35 (2010) 2025–2032.
[40] H. Senoh, N. Takeichi, H.T. Takeshita, H. Tanaka, T. Kiyobayashi, N. Kuriyama, Mater. Trans. 44 (2003) 1663–1666.